PCCP

Cite this: *Phys. Chem. Chem. Phys.*, 2011, **13**, 20155–20161

www.rsc.org/pccp

PAPER

Mesoporous TiO_2 nanostructures: a route to minimize Pt loading on titania photocatalysts for hydrogen production

Tarek A. Kandiel,[ab] Adel A. Ismail[ac] and Detlef W. Bahnemann*[a]

Received 15th August 2011, Accepted 1st September 2011
DOI: 10.1039/c1cp22612f

Mesostructured TiO_2 nanocrystals have been prepared using Pluronic F127 as the structure-directing agent. Platinum nanoparticles at different contents (0.1–1.0 wt%) have been photochemically deposited onto the mesoporous TiO_2. TEM investigation of 0.2 wt% Pt/TiO_2 calcined at 450 °C reveals that the TiO_2 particles are quite uniform in size and shape with the particle sizes of TiO_2 and Pt being 10 and 3 nm, respectively. The photocatalytic activities of the Pt loaded TiO_2 have been assessed and compared with those of nonporous commercial Pt/TiO_2-P25 by determining the rates and the photonic efficiencies of molecular hydrogen production from aqueous methanol solutions. The results show that the amount of hydrogen evolved on Pt/TiO_2-450 at low Pt loading (0.2 wt%) is three times higher than that evolved on Pt/TiO_2-P25 and twelve times higher than that evolved on Pt/TiO_2-350. Despite the BET surface area of the TiO_2-450 photocatalyst being 3.5 times higher than that of TiO_2-P25, a 60% smaller amount of the Pt co-catalyst is required to obtain the optimum photocatalytic hydrogen production activity. The reduced Pt loading on the mesoporous TiO_2 will be important both from a commercial and an ecological point of view.

1. Introduction

Hydrogen is the most common element on earth, but it does not occur to any significant extent in its elemental form. It is mostly present in water, in biomass, and in hydrocarbons. Hydrogen gas is currently produced from a variety of primary sources, such as natural gas, naphtha, heavy oil, methanol, biomass, wastes, coal, solar energy, wind energy, hydropower, and nuclear energy.[1,2] It is a clean source of energy fuel because the chemical energy stored in the H–H bond can be released in a controlled way when it combines with oxygen, yielding only water as the reaction product. Accordingly, a future energy infrastructure based on H_2 is regarded as an ideal long-term solution to solve energy-related environmental problems. There is no doubt that hydrogen has the potential to provide a clean and affordable energy supply that can minimize our dependence on oil and therefore enhance the global economy and reduce environmental pollution.

In view of the high energy demand and the complexity associated with all reforming processes, it is of considerable interest to explore photocatalysis as an alternative technology for H_2 production from water and/or biomass derived compounds such as methanol.[3] One of the most important limitations for the applications of photocatalysis for water decomposition is that employing pure water in this process is still rather inefficient.[4,5] This is related to the fact that the simultaneous reduction and oxidation of water is a complex multistep reaction involving four electrons. Using sacrificial donors such as methanol can improve remarkably the H_2 production,[6,7] as holes are scavenged by these molecules and charge carrier recombination can be greatly reduced. Furthermore, as O_2 is not produced, the back reaction to produce water is suppressed, increasing the H_2 yield.

Because of its availability, its stability, and its non-toxicity TiO_2 has been proposed to be the most suitable photocatalyst up to now. However, bare TiO_2 is not able to catalyze the H_2 evolution even in the presence of methanol. In the presence of an electron donor, such as methanol, and in the absence of O_2, the excess holes will be consumed and the photogenerated electrons will be trapped near the surface forming trivalent titanium (Ti^{3+}) instead of reducing H^+.[8] Loading the TiO_2 surface with small noble metal islands creates sinks for the electrons as well as active sites for the H_2 formation, thus facilitating the separation of e^-/h^+ pairs photogenerated in TiO_2 and promoting the formation of H_2 gas.[9–11] The photocatalytic activity of hydrogen evolution from aqueous methanol solutions over TiO_2 depends strongly on the presence of noble metal co-catalysts deposited on the semiconductor surface as well as on various physicochemical properties of TiO_2.

[a] *Photocatalysis and Nanotechnology Unit, Institut für Technische Chemie, Leibniz Universität Hannover, Callinstrasse 3, D-30167 Hannover, Germany. E-mail: bahnemann@iftc.uni-hannover.de*
[b] *Department of Chemistry, Faculty of Science, Sohag University, Sohag 82524, Egypt*
[c] *Nanostructured & Nanotechnology Division, Advanced Materials Department, Central Metallurgical Research and Development Institute (CMRDI), P.O. Box: 87 Helwan, Cairo 11421, Egypt*

In general, modification of TiO_2 with noble metals has been reported to be a very effective method for the enhancement of its photocatalytic activity.[12] Among these noble metals, Pt modified TiO_2 has usually shown the best photocatalytic activity, particularly, for hydrogen production from aqueous methanol solutions.[13,14] Hence, as concluded from the work functions of TiO_2 (4.6–4.7 eV) and Pt (5.36–5.63 eV),[15] the Fermi level of the Pt metal is more positive than that of TiO_2, the photo-excited electrons can be readily transferred from the TiO_2 conduction band to the Pt particles deposited on its surface, while photo-generated valence band holes remain on the TiO_2. The electron transfer to the metal islands will greatly reduce the probability of electron–hole recombination, resulting in a more efficient electron/hole separation and thus in enhanced photocatalytic activities.

However, while Pt co-catalysts have shown the highest activity for hydrogen production from aqueous methanol solutions, their cost is still one of the limitations for the practical application of Pt-loaded TiO_2 photocatalysts for hydrogen production. Thus, the research for TiO_2 nanostructures exhibiting high photocatalytic activities and at the same time requiring only small amounts of Pt co-catalyst is of great interest. Herein, we present the results of a study focused on the synthesis of mesoporous TiO_2 nanostructures as improved design of TiO_2 photocatalysts exhibiting high photocatalytic activity and at the same time requiring a reduced amount of the Pt co-catalyst to achieve the optimum hydrogen generation rate.

2. Experimental

Materials

The block copolymer surfactant EO_{106}–$PO_{70}EO_{106}$ (F-127, EO = $-CH_2CH_2O-$, PO = $-CH_2(CH_3)CHO-$, M_w 12 600 g mol^{-1}), $Ti(OC(CH_3)_3)_4$ (TBOT), HCl, C_2H_5OH, and CH_3COOH, hexachloroplatinic acid hexahydrate were purchased from Sigma-Aldrich and used as received. All aqueous solutions were prepared with deionized water from a SARTORIUS ARIUM 611 apparatus (resistivity = 18.2 MΩ cm).

Synthesis of mesoporous TiO_2

Highly ordered TiO_2 nanocrystals were synthesized through a simple one-step sol–gel process in the presence of the F127 triblock copolymer as a structure directing agent. To minimize possible variables, the molar ratio of each reagent in the starting solution was fixed at TiO_2/F127/C_2H_5OH/HCl/CH_3COOH = 1 : 0.02 : 50 : 2.25 : 3.75. In a typical preparation, 1.6 g of F127, 2.3 ml of CH_3COOH and 0.74 ml of HCl were dissolved in 30 ml of ethanol and then added to 3.5 ml of TBOT.[16] The mixture was stirred vigorously for 60 min and transferred into a Petri dish. Ethanol was subsequently evaporated at 40 °C and a relative humidity of 40% for 12 h followed by the transfer of the sample into a 65 °C oven and ageing for an additional 24 h. The as-made mesostructured hybrids were calcined at 350–450 °C in air for 4 h at a heating rate of 1 °C min^{-1} and a cooling rate of 2 °C min^{-1} to remove the surfactant and to obtain mesostructured TiO_2 denoted as TiO_2-350, TiO_2-400, and TiO_2-450.

Photodeposition of Pt onto mesoporous TiO_2

Pt islands were photochemically deposited onto mesoporous TiO_2 as follows: 0.5 g of mesoporous TiO_2 was suspended by stirring in 100 ml aqueous solution containing specific concentrations of H_2PtCl_6 to obtain varied (*i.e.*, 0.1–1.0 wt%) Pt loaded TiO_2 photocatalysts. The resulting solution was irradiated with UV(A) light employing a Philips fluorescence Hg lamp (illumination intensity: 1.0 mW cm^{-2}) for 2 h under an Ar atmosphere. Afterwards, 1 ml methanol was injected into the solution followed by further illumination for 10 h. The obtained powder was separated by centrifugation, washed with water, and dried at 110 °C for 12 h. The Pt photochemically deposited onto mesoporous TiO_2-350, TiO_2-400, and TiO_2-450 was labelled as Pt/TiO_2-350, Pt/TiO_2-400, and Pt/TiO_2-450 respectively.

Characterization

Transmission electron microscopy (TEM) was conducted at 200 kV with a JEOL JEM-2100F-UHR field-emission instrument equipped with a Gatan GIF 2001 energy filter and a 1k-CCD camera in order to obtain EEL spectra. Wide angle X-ray diffraction (WXRD) data were acquired employing a Bruker AXS D4 Endeavour X diffractometer using Cu $K\alpha_{1/2}$, $\lambda_{\alpha1}$ = 154.060 pm, $\lambda_{\alpha2}$ = 154.439 pm radiation with small angle X-ray diffraction (SXRD) patterns being recorded on a Bruker D8 advance. The nitrogen adsorption and desorption isotherms at 77 K were measured using a Quantachrome Autosorb 3B after the samples were vacuum-dried at 200 °C overnight. The sorption data were analyzed using the Barrett–Joyner–Halenda (BJH) model with the Halsey equation.[17]

Photocatalytic activity measurements

The photocatalytic molecular hydrogen production tests were performed in a double jacket Duran glass reactor (110 cm^3) with three outlets as described elsewhere.[18,19] In a typical run, 0.0375 g of the modified TiO_2 photocatalysts were suspended in 75 ml of an aqueous methanol solution (0.03 M) by sonication. The suspension was transferred to the photoreactor and bubbled with Ar for 30 min to remove dissolved O_2. The reactor was sealed with a silicone rubber septum and repeatedly flushed with Ar for another 30 min until no O_2 and N_2 were detected by gas chromatography in the headspace above the solution. Subsequently, the stopcocks were closed and the photoreactor was connected to the cooling system. The photoreactor was irradiated from the outside using an Osram XBO 1000 W Xenon lamp in a Müller LAX 1000 lamp housing. The evolved gas was sampled at a constant rate through the silicone rubber septum by using a locking-type syringe. The sampled gas was quantitatively analyzed using a gas chromatograph (Shimadzu 8A, TCD detector). The GC was equipped with a molecular sieve 5 Å packed column for hydrogen analysis. Ar was used as the carrier gas.

3. Results and discussions

3.1. Photocatalyst synthesis and characterization

Well-ordered mesostructured TiO_2 nanocrystals were prepared using Pluronic F127 as the structure-directing agent.

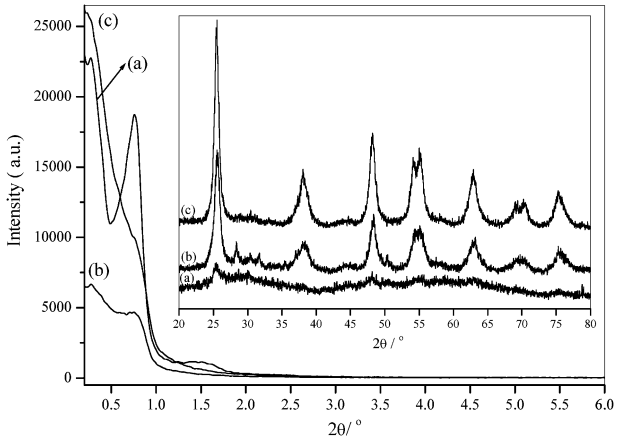

Fig. 1 SAXS patterns of two-dimensional hexagonal mesoporous Pt photodeposited on TiO_2 nanoparticles calcined at 350 (a), 400 (b) and 450 °C (c). Inset, WXRD of Pt photodeposited on TiO_2 nanocomposites calcined at 350 (a), 400 (b) and 450 °C (c) for 4 h. Shifted for the sake of clarity.

The preparation of the mesostructured TiO_2 involved the alcoholysis of TBOT by ethanol in the presence of amphiphilic block copolymers and acetic acid. Cross-linking of the inorganic network under these conditions occurred, through the slow hydrolysis of the titanium species by the humidity of the surrounding atmosphere. Nanosized metal-oxo-acetate particles form rapidly in the acetic acid solution. These nanoparticles are quite stable and grow slowly due to the slow introduction of water from the ambient environment and the esterification of acetic acid.[20] The obtained gel samples were calcined to produce TiO_2-350, TiO_2-400 and TiO_2-450, respectively. Then, Pt was photochemically deposited onto the mesoporous TiO_2-350, TiO_2-400 and TiO_2-450 yielding Pt/TiO_2-350, Pt/TiO_2-400, and Pt/TiO_2-450, respectively. The small angle X-ray scattering (SAXS) patterns of the mesoporous Pt/TiO_2-350, Pt/TiO_2-400, and Pt/TiO_2-450 are shown in Fig. 1. Pt/TiO_2-350 shows two well-resolved peaks, which can be indexed to the (10) and (20) Bragg reflections confirming an ordered 2D-hexagonal mesostructure of the *P6m* space group. The observed high intensities and the sharpness of the peaks prove that a long-range order exists in the Pt/TiO_2-350 nanoarchitectures. With increasing calcination temperature, the diffraction peaks are becoming weaker with the (10) and (20) reflections indicating that the long-range ordering of the mesopores is already disappearing for the Pt/TiO_2-450 sample. In general, well ordered 2D-hexagonal TiO_2 nanoparticles were found to be stable up to 350 °C. After template removal, the structural regularity declines with increasing temperature from 350 to 450 °C but the lattice parameters calculated from the d_{10} value decrease only from 12.96 to 11.45 nm indicating an approx. 11.8% contraction of the structure at 450 °C. It is evident that after the collapses of the hexagonal ordering even the pore channels themselves start to collapse and disordered mesostructures of crystalline TiO_2 are obtained at 450 °C. Wide angle XRD reflections (Fig. 1, inset) showed that the Pt/TiO_2-350 sample exhibits low intensity and rather broad peaks evincing, however, that the TiO_2 particles already exist in the anatase phase. It is obvious that the XRD reflections show a gradual increase and a narrowing in the anatase-TiO_2 (101) peaks (2θ = 25.4°) with increasing calcination temperature. The peaks characteristic for the (101), (004), (200), (211) and (213) lattice planes can also be identified evincing that the TiO_2 phase easily nucleates during heating and already upon calcination at 350 °C transforms into nanocrystals. This is explained by the amorphous-anatase TiO_2 transition and the subsequent growth of anatase-TiO_2 particles. Analyzing the width at half maximum of the reflections employing Scherrer's equation[21] results in TiO_2 nanocrystal sizes with a maximum of 8 nm at 450 °C (see Table 1). Interestingly, no crystalline Pt phase is detected. Thus, at low Pt content a high dispersion of smaller nanoparticles of Pt onto the surface and the pores has obviously been achieved.

In the N_2 adsorption/desorption studies large hysteresis loops resembling typical H_2-type isotherms are observed for 0.2 wt% Pt loaded TiO_2-350, TiO_2-400 and TiO_2-450 (Fig. 2). The sharpness of the inflection resulting from capillary condensation at relative pressures p/p_0 between 0.45 and 0.75 is characteristic for mesopores ordered in two-dimensional hexagonal symmetry. The Barrett–Joyner–Halenda (BJH) analysis shows that the 0.2 wt% Pt loaded TiO_2-450 mesoporous network exhibits mean pore sizes of about 6.53 nm (Fig. 2, inset), but also demonstrates that the pore size distribution is quite narrow. The mesoporous Pt/TiO_2-350 possesses high surface areas of 267 m^2 g^{-1} and large pore volumes of 0.32 cm^3 g^{-1}; they are reduced to 175 m^2 g^{-1} and 0.29 cm^3 g^{-1}, respectively, for the Pt/TiO_2-450 sample as a result of the calcination at 450 °C (Table 1). The BET surface areas, the pore volumes, and the pore diameters of all samples are summarized in Table 1. The slight decrease in pore size with increasing calcination temperature up to 450 °C reveals that the thickness of the pore walls increases concomitantly from 6.5 to 6.8 nm. The wall thickness is found to be slightly smaller for the sample calcined at 450 °C, implying that some of the TiO_2 nanocrystals could partially pierce even into the

Table 1 Textural properties of Pt photodeposited onto/TiO_2 calcined at 350, 400, and 450 °C and Pt photodeposited onto commercial TiO_2-P25 and their photocatalytic properties

Photo-catalysts	S_{BET}/m^2 g^{-1}	P_{TiO_2}/nm	d_{100}/nm	Unit cell size/nm	Pore wall/nm	ζ/%	V_p/cm^3 g^{-1}	D_p/nm
TiO_2 a. m.	—	—	12.96	14.98	—	—	—	—
TiO_2-350	267	3.5	11.87	13.71	6.5	0.45	0.31	7.21
TiO_2-400	209	6	11.57	13.48	6.7	4.0	0.30	6.78
TiO_2-450	175	8	11.45	13.23	6.7	5.35	0.29	6.53
TiO_2-P25	50	—	—	—	—	1.8	—	—

S_{BET}: surface area, $P_{S\ TiO_2}$: average particle size of TiO_2 nanoparticle, ζ: photonic efficiency, V_p: pore volume, D_p: pore diameter.

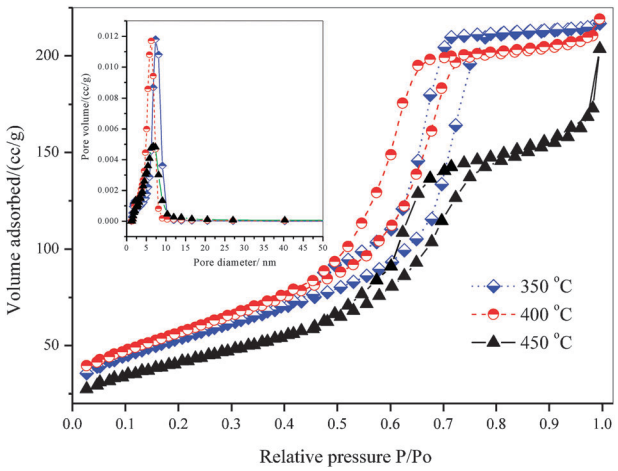

Fig. 2 N_2 sorption isotherms and pore size distributions (inset) of mesoporous 0.2 wt% Pt loaded TiO_2 calcined at 350, 400 and 450 °C for 4 h.

channel space,[22] which is particularly evident from the HRTEM images (Fig. 3f).

The TEM images of the mesoporous Pt/TiO_2-350 (Fig. 3a and b) show a well-defined 2D hexagonal mesostructure, evincing the formation of a highly ordered mesostructure,[23] which is consistent with the analysis of the SAXS pattern (Fig. 1a). Already upon calcination at 350 °C the TiO_2 nanocrystals are randomly oriented within the amorphous walls as indicated by the characteristic lattice fringes (Fig. 3a).

The TEM images of the mesoporous 0.2 wt% Pt/TiO_2-400 and 0.2 wt% Pt/TiO_2-450 demonstrate that the TiO_2 nanoparticles are not agglomerated and quite uniform in size and shape (Fig. 3c and d). The dark-field TEM image of Pt/TiO_2-450 (Fig. 3e) clearly shows that the Pt nanoparticles are well dispersed exhibiting diameters of ~3 nm. The selected area electron diffraction (SAED) pattern analysis (Fig. 3a and f inset) further confirms that anatase is progressively formed with its particle size increasing from 5 to 10 nm with increasing calcination temperatures from 350 to 450 °C. Both, the HRTEM image (Fig. 3f) and the selective area electron diffraction (SAED, inset of Fig. 3f) show well resolved (101) lattice fringes (distance: 0.352 nm) and diffraction cycles indicative of a highly crystalline TiO_2 anatase framework.

3.2. H_2 production from aqueous methanol solutions

The photocatalytic activities of the Pt loaded photocatalysts have been assessed and compared with that of nonporous commercial Pt/TiO_2 P25 by determining the rates and the photonic efficiencies of molecular hydrogen production from aqueous methanol solutions. The hydrogen evolution on bare TiO_2 was negligible under the applied experimental conditions. In order to optimize the amount of Pt required for higher photocatalytic activity, the TiO_2 sample calcined at 450 °C (TiO_2-450) has been loaded with different amounts of Pt using the photochemical deposition method. The Pt/TiO_2-450 sample has been chosen due to its higher crystallinity and its superior mesoporous structure. Even though Pt/TiO_2-350 and Pt/TiO_2-400 already show ordered mesoporous structures,

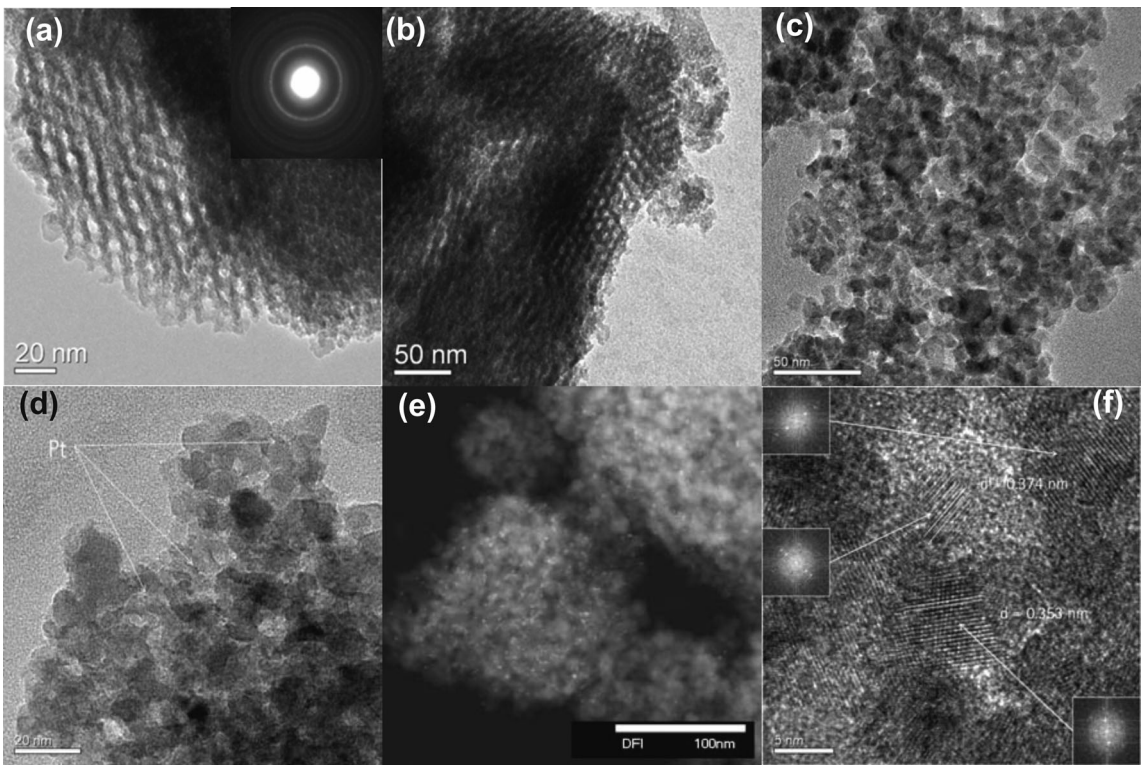

Fig. 3 TEM images of two-dimensional hexagonal mesoporous Pt loaded TiO_2 nanocomposites calcined at 350 (a and b), 400 (c) and 450 °C (d). The insets show the SAED patterns for the anatase phase at 350 (a) and 450 °C (f). Dark-field TEM image of Pt loaded TiO_2 at 450 °C (e) and HRTEM image of TiO_2 anatase phase using (101) (f).

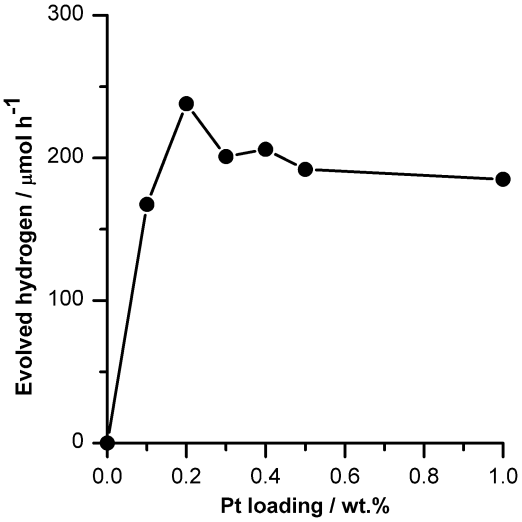

Fig. 4 Rate of hydrogen evolution on TiO_2-450 photocatalyst loaded with different amounts of Pt co-catalyst upon UV(A) illumination (60 mW cm^{-1}).

preliminary results had shown that they exhibit smaller photocatalytic activities than Pt/TiO_2-450. Fig. 4 shows the rate of hydrogen evolution from aqueous methanol solutions on TiO_2-450 photocatalysts loaded with different amounts of the Pt co-catalyst. Interestingly, the 0.2 wt% Pt loaded TiO_2-450 exhibits the highest activity. Usually, the optimum amount of Pt loading on Evonik TiO_2 P25, which is a well known photocatalyst and usually has been recommended as a reference photocatalyst,[24] is 0.5 wt%.[11,25] The ratio of Pt loading on TiO_2 P25 has also been found under the applied experimental conditions. Despite the BET surface area of TiO_2-450 photocatalyst being 3.5 times higher than that of TiO_2-P25, it needs a 60% smaller amount of Pt co-catalyst to exhibit optimum photocatalytic hydrogen production activity. This finding is important both from a commercial and an ecological point of view.

Fig. 5 shows the time course of molecular hydrogen production on the different 0.2 wt% Pt loaded TiO_2 photocatalysts

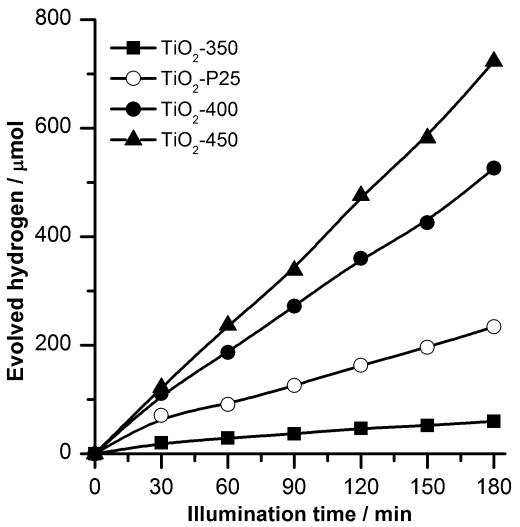

Fig. 5 Time course of hydrogen evolution over 0.2 wt% Pt loaded photocatalysts upon UV(A) illumination (60 mW cm^{-1}).

(TiO_2-350, TiO_2-400, TiO_2-450 and TiO_2-P25) from aqueous methanol solutions upon UV(A) illumination. The photonic efficiencies (ζ) of hydrogen evolution have been calculated by dividing the rate of hydrogen evolution by the photon flux ($\zeta = R/I_0$).[26] The rate of hydrogen evolution has been calculated from the slope of the time course of the hydrogen production. The photon flux has been calculated from the intensity of UV(A) light at the entrance window of the photoreactor as measured by a UV light meter (ultraviolet radiometer LTLutron UVA-365) to be 4.42×10^3 μeinstein h^{-1}. The calculated photonic efficiency values for all investigated photocatalysts are given in Table 1. The results show that the amount of hydrogen evolved on Pt/TiO_2-450 is three times higher than that evolved on Pt/TiO_2-P25 and twelve times higher than that evolved on Pt/TiO_2-350. However, the latter has highly ordered mesoporous structures (see Fig. 1a and 3a) and also a higher surface area (see Table 1). These results clearly indicate that the crystallinity of TiO_2 is an important factor greatly affecting the rate of hydrogen evolution. A high degree of crystallinity is apparently more important than a high surface area for hydrogen production. In a photocatalytic system the recombination between photogenerated electrons and holes presents a serious problem limiting its overall efficiency. The increase of crystallinity is expected to lead to a decrease of the number of defect sites and hence to a decrease of the recombination rate.[5]

In order to explain why the TiO_2-450 photocatalyst needs a smaller amount of the Pt co-catalyst than TiO_2-P25, to exhibit higher photocatalytic activity, the ratio of the number of Pt nanoparticles to TiO_2 nanoparticles has been calculated. Assuming that Pt nanoparticles are spherical and have a diameter of 3.0 nm (see Fig. 3e), the volume of one 3.0 nm Pt nanoparticle is calculated to be 1.41×10^{-20} cm^3. Considering that the mass density of Pt is 21.4 g cm^{-3}, the average weight of one Pt nanoparticle is derived to be approximately 3.02×10^{-19} g. Therefore, the number of Pt islands for each gram of 0.2 wt% Pt-loaded TiO_2 will be 6.61×10^{15}. Assuming spherical TiO_2 nanoparticles with 8 nm average diameter (see Table 1) and a mass density of 3.9 g cm^{-3}, the number of TiO_2 nanoparticles per gram is calculated to be 9.57×10^{17}. Thus, the number of Pt nanoparticles per TiO_2-450 nanoparticle should be 1 Pt particle for 145 TiO_2 particles. By the same way, the number of Pt particles per TiO_2-P25 particle has been calculated to be 1 Pt particle for 30 TiO_2-P25 particles, assuming that the average particle size of TiO_2-P25 is 25 nm. However, it should be mentioned that TiO_2-P25 is a mixture of anatase and rutile particles with the particle size of rutile being larger than that of anatase.[27] Assuming that the Pt nanoparticles are the only active centers available for hydrogen evolution, it can be concluded from these simple calculations that the photogenerated electrons are transferred through a three-dimensional network of TiO_2 nanoparticles to reach the Pt nanoparticles where the hydrogen evolution will be catalyzed as schematically shown in Fig. 6. This model appears to be responsible because the bare TiO_2 surface, on the one hand, cannot be considered as an active surface for hydrogen evolution as experimentally confirmed and, on the other hand, there is no molecular oxygen available to act as an electron acceptor regardless of the presence or absence of the Pt co-catalyst.

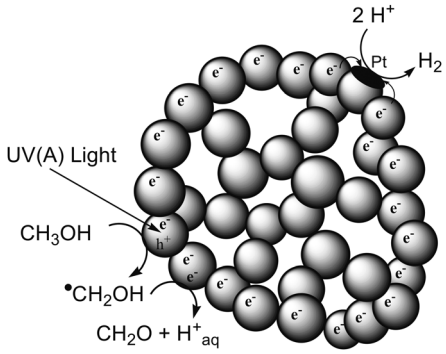

Fig. 6 Schematic illustration of the proposed pathway of electron transfer to explain the high activity of mesoporous nanostructures for hydrogen production from aqueous methanol solutions on Pt loaded TiO_2 photocatalyst under small Pt nanoparticles to TiO_2 nanoparticles ratio.

It is obvious from the nitrogen absorption measurements that TiO_2-450 has a mesoporous structure whereas TiO_2-P25 is a nonporous material. This mesoporous structure can thus provide suitable interfaces for a facile interparticle charge transfer while the reactants can freely diffuse through the pores.[25,28,29] While the excited TiO_2 nanoparticle can transfer the absorbed energy through the mesoporous TiO_2 network to other ground-state TiO_2 particles, the probability of the hole trapping at the surface hydroxyl group forming an adsorbed hydroxyl radical that is subsequently transferred to an adsorbed CH_3OH molecule is considered to be high. Consequently, the probability of electron transfer to the Pt particle is increased by an increased CH_3OH diffusion through the pores of the nanostructures. This might explain why TiO_2-450 which has a mesoporous structure requires a small amount of Pt loading while, however, having a higher surface area than TiO_2-P25. These findings are in agreement with the so-called antenna mechanism recently proposed by Bahnemann *et al.*[30,31] and with the recent finding that the mesoporous TiO_2 structures with highly interconnected nanograins result in favourable conduction pathways for electrons without using conductive thin layers. Improving the charge collection during lithium storage at high rates, moreover, the porous structure favours the complete wetting of the TiO_2 by the liquid electrolyte so that the Li^+ insert/extraction can be achieved.[32]

4. Conclusions

Platinum nanoparticles at different contents (*i.e.*, 0.1–1.0 wt%) have been photochemically deposited onto mesoporous TiO_2. The loading of small amounts of Pt (0.2 wt%) into the mesoporous TiO_2 network has been found to be sufficient to enhance the photonic efficiencies. 0.2 wt% Pt loaded onto mesoporous TiO_2 (Pt/TiO_2-450) exhibits a photonic efficiency of hydrogen production from aqueous methanol solutions that is three times higher than that of Pt loaded TiO_2-P25. It was also found that Pt/TiO_2-450 is more active than Pt/TiO_2-350 while, however, the latter has a higher surface area than the former, revealing that a high degree of crystallinity is more important than a high surface area for optimum photocatalytic hydrogen production. The increase of the crystallinity leads to a decrease in the number of defect sites and hence a decrease of the charge carriers recombination. In general, the advantage of using mesoporous TiO_2-450 is to minimize the amount of Pt cocatalyst loading required for molecular hydrogen production from aqueous methanol solutions. The key to this success is the preparation of Pt/TiO_2 networks with mesoporous nanostructures which at the same time render the methanol diffusion into the bulk of the photocatalysts and it hence provides fast transport channels for the methanol molecules and facilitates the charge carrier separation. Therefore, it should be possible to apply smart molecular engineering approaches to design photocatalytic systems exhibiting considerably higher photonic efficiencies than existing systems through using TiO_2 mesoporous nanostructured photocatalysts which even needs little amount of Pt cocatalyst in comparison with the commercially available photocatalyst TiO_2 P25.

Acknowledgements

Financial support from the Bundesministerium für Bildung und Forschung (BMBF) is gratefully acknowledged (Grant No. 60420819). A. A. Ismail acknowledges the Alexander von Humboldt (AvH) Foundation for granting him a research fellowship.

Notes and references

1 R. M. Navarro, M. C. Sanchez-Sanchez, M. C. Alvarez-Galvan, F. del Valle and J. L. G. Fierro, *Energy Environ. Sci.*, 2009, **2**, 35–54.
2 R. M. Navarro, M. A. Pena and J. L. G. Fierro, *Chem. Rev.*, 2007, **107**, 3952–3991.
3 C. N. Hamelinck and A. P. C. Faaij, *J. Power Sources*, 2002, **111**, 1–22.
4 K. Maeda and K. Domen, *J. Phys. Chem. Lett.*, 2010, **1**, 2655–2661.
5 A. Kudo and Y. Miseki, *Chem. Soc. Rev.*, 2009, **38**, 253–278.
6 T. Kawai and T. Sakata, *Nature*, 1980, **286**, 474–476.
7 T. Kawai and T. Sakata, *J. Chem. Soc., Chem. Commun.*, 1980, 694–695.
8 D. Bahnemann, A. Henglein, J. Lilie and L. Spanhel, *J. Phys. Chem.*, 1984, **88**, 709–711.
9 D. Bahnemann, A. Henglein and L. Spanhel, *Faraday Discuss.*, 1984, **78**, 151–163.
10 C. Y. Wang, R. Pagel, D. W. Bahnemann and J. K. Dohrmann, *J. Phys. Chem. B*, 2004, **108**, 14082–14092.
11 J. Kiwi and M. Gratzel, *J. Phys. Chem.*, 1984, **88**, 1302–1307.
12 M. Ni, M. K. H. Leung, D. Y. C. Leung and K. Sumathy, *Renewable Sustainable Energy Rev.*, 2007, **11**, 401–425.
13 G. R. Bamwenda, S. Tsubota, T. Nakamura and M. Haruta, *J. Photochem. Photobiol., A*, 1995, **89**, 177–189.
14 T. Sreethawong and S. Yoshikawa, *Catal. Commun.*, 2005, **6**, 661–668.
15 S. L. Lee, J. Scott, K. Chiang and R. Amal, *J. Nanopart. Res.*, 2009, **11**, 209–219.
16 F. Jie, S. W. Boettcher and G. D. Stucky, *Chem. Mater.*, 2006, **18**, 6391–6396.
17 S. J. Gregg and K. S. W. Sing, *Adsorption, surface area and porosity*, Academic Press, London, 1982.
18 T. A. Kandiel, R. Dillert and D. W. Bahnemann, *Photochem. Photobiol. Sci.*, 2009, **8**, 683–690.
19 T. A. Kandiel, A. Feldhoff, L. Robben, R. Dillert and D. W. Bahnemann, *Chem. Mater.*, 2010, **22**, 2050–2060.
20 U. Schubert, *J. Mater. Chem.*, 2005, **15**, 3701–3715.
21 L. V. Azároff and M. J. Buerger, *The powder method in X-ray crystallography*, New York, 1958.
22 R. Liu, Y. Ren, Y. Shi, F. Zhang, L. Zhang, B. Tu and D. Zhao, *Chem. Mater.*, 2008, **20**, 1140–1146.

23 Y. Peidong, D. Tao, Z. Dongyuan, F. Pingyun, D. Pine, B. F. Chmelka, G. M. Whitesides and G. D. Stucky, *Science*, 1998, **282**, 2244–2246.
24 B. Ohtani, *Chem. Lett*., 2008, 217–229.
25 N. Lakshminarasimhan, E. Bae and W. Choi, *J. Phys. Chem. C*, 2007, **111**, 15244–15250.
26 N. Serpone, R. Terzian, D. Lawless, P. Kennepohl and G. Sauve, *J. Photochem. Photobiol., A*, 1993, **73**, 11–16.
27 T. Ohno, K. Sarukawa, K. Tokieda and M. Matsumura, *J. Catal*., 2001, **203**, 82–86.
28 N. Lakshminarasimhan, W. Kim and W. Choi, *J. Phys. Chem. C*, 2008, **112**, 20451–20457.
29 X. Chen, X. Wang and X. Fu, *Energy Environ. Sci*., 2009, **2**, 872–877.
30 A. A. Ismail, D. W. Bahnemann, I. Bannat and M. Wark, *J. Phys. Chem. C*, 2009, **113**, 7429–7435.
31 C. Y. Wang, R. Pagel, J. K. Dohrmann and D. W. Bahnemann, *C. R. Chim*., 2006, **9**, 761–773.
32 K. Saravanan, K. Ananthanarayanan and P. Balaya, *Energy Environ. Sci*., 2010, **3**, 939–948.